A Letters Journal Exploring the Frontiers of Physics

October 2019

EPL, **128** (2019) 14002
doi: 10.1209/0295-5075/128/14002

www.epljournal.org

Barrier bucket and transversely split beams for loss-free multi-turn extraction in synchrotrons

M. Vadai[1,2(a)], A. Alomainy[2], H. Damerau[1], S. Gilardoni[3], M. Giovannozzi[1] and A. Huschauer[1]

[1] *Beams Department, CERN - 1211 Geneva 23, Switzerland*
[2] *Queen Mary University of London - London E1 4NS, UK*
[3] *Engineering Department, CERN - 1211 Geneva 23, Switzerland*

received 26 March 2019; accepted in final form 16 September 2019
published online 20 November 2019

PACS 41.75.Lx – Other advanced accelerator concepts
PACS 29.27.Bd – Beam dynamics; collective effects and instabilities
PACS 05.45.-a – Nonlinear dynamics and chaos

Abstract – A special radio-frequency manipulation has been studied and successfully implemented at the CERN Proton Synchrotron for the first time. This technique aims at depleting a well-defined fraction of a continuous longitudinal beam distribution by creating a so-called barrier bucket. In addition to the intrinsic interest for its originality, this approach has an immediate application at CERN in combination with the Multi-Turn Extraction scheme. The combination of these two exotic techniques into a single, highly sophisticated process allows to dramatically reduce the beam loss at PS extraction, thus opening the door to the production of high-intensity proton beams for future fixed-target experiments at the CERN Super Proton Synchrotron.

Introduction. – Since the introduction of the Multi-Turn Extraction (MTE) as an operational beam manipulation in the CERN Proton Synchrotron (PS), the losses of high-intensity proton beams delivered to the fixed-target physics facilities at the CERN Super Proton Synchrotron (SPS) have been greatly reduced [1–5] with respect to the previously applied Continuous Transfer (CT) extraction method [6,7]. MTE is a technique based on beam splitting in the transverse horizontal plane by means of trapping particles into stable resonance islands generated by non-linear magnetic fields, such as sextupoles and octupoles [1,8,9]. Although the losses in the transverse plane have been cured by this new extraction technique, residual losses originate from the fact that the SPS requires the beam from the PS to be debunched and modulated with a 200 MHz structure prior to extraction. During the extraction process, fast dipoles, which are also referred to as kickers in the following, are used to deflect the beam out of the PS ring. The residual losses are generated during the rise time of these kickers, as particles are swept through the blade of the magnetic extraction septum, where they are eventually lost. These losses lead to local irradiation of accelerator equipment and consequently issues in terms of hands-on maintenance and increased failure rate. A sketch of the extraction scheme is shown in fig. 1.

In order to mitigate these losses, a so-called dummy septum [10–14] has been developed and installed in the ring (a layout of the PS ring with the main elements used for the studies described in this paper is shown in fig. 2). This well-shielded passive device is made to intercept the particles during the rise time of the fast dipoles, thus shadowing the blade of the magnetic extraction septum.

The most efficient approach to further reduce the extraction losses is to create a gap in the longitudinal beam distribution, which has to be synchronised with the rise time of the kicker magnets. If the duration of the longitudinal gap matches the rise time of the extraction elements, the beam losses can be virtually reduced to zero. Such a gap can be generated by means of special radio-frequency (RF) gymnastics, which have been applied for the first time in the PS ring in the framework of this study.

(a) E-mail: mihaly.vadai@cern.ch (corresponding author)

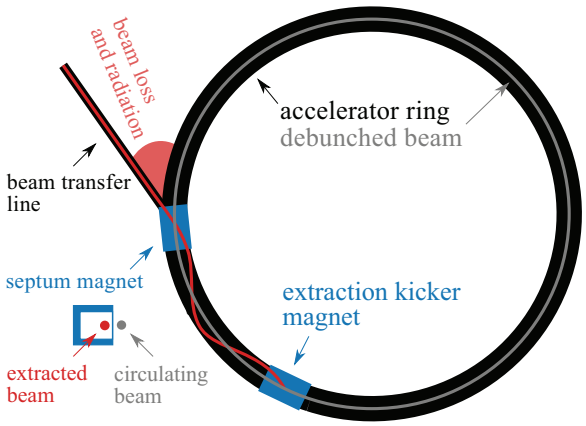

Fig. 1: Sketch of the principle of beam extraction with the beam losses induced by the continuous longitudinal distribution. The rise time of the kickers is of the order of 390 ns, referring to the time needed to increase the kicker strength from 5% to 95% of the nominal value (one PS turn corresponds to 2.1 μs).

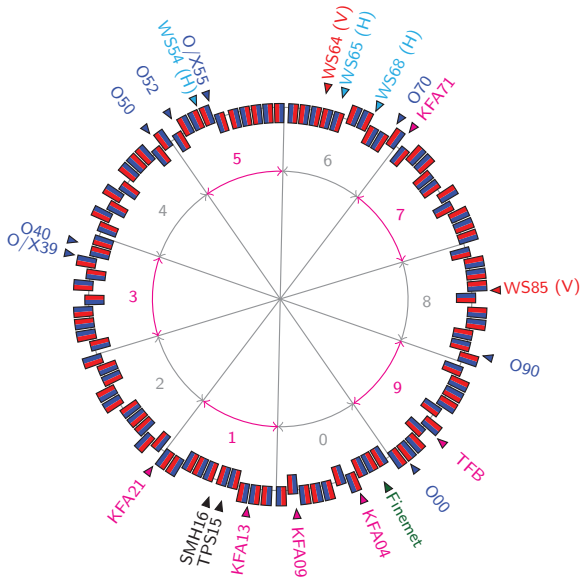

Fig. 2: Layout of the PS ring including the combined-function main magnets (red and blue rectangles for the focusing and defocusing parts, respectively, where the radial offset between the rectangles accounts for the four different magnet types [24]) and the location of the key elements for MTE: sextupoles and octupoles (element names starting with X or O), fast dipoles for beam extraction (element names starting with K), magnetic (SMH16) and dummy (TPS15) septa, and wire scanners (element names starting with W) for the measurement of the transverse beam distributions. The position of the Finemet® cavity [25] used for the generation of the barrier bucket is also indicated.

The barrier bucket manipulation alone or the acceleration with pulsed RF systems has been performed routinely in different laboratories [15–19] and some of the applications also include purposes of loss reduction for single-turn extraction. MTE is also part of the routine operation of the PS machine [4] since the end of 2015 [2]. However, the combination of both techniques with the associated reduction of extraction losses has been successfully demonstrated for the first time. Note that this implies mastering two sophisticated techniques, which, in principle, are not fully decoupled. Their combination has shown that the barrier bucket manipulation preserves the transverse beam quality. Compared to the conventional debunching, the longitudinal distribution is only altered close to the barriers. Furthermore, clear intensity-dependent effects (see, *e.g.*, [20,21] for the case of transverse splitting) have been observed in the past, but in spite of this, the novel technique has provided excellent results independently of the beam intensity used. Thanks to the new scheme, new options become viable for future operation of fixed-target beams in the CERN accelerator chain. Hence, combining MTE with the barrier bucket manipulation allows to extend the performance reach of the fixed-target physics programme at the SPS, possibly enabling novel physics searches as studied by the CERN Physics Beyond Colliders (PBC) working group [22,23].

Particle dynamics in a barrier bucket. – The electric potential generated by RF fields is suitable to confine the charged beam particles into several stable regions, called buckets, created by the RF cavities typically using a sinusoidal waveform, whose frequency is an integer harmonic of the synchrotron revolution frequency. Thus, the RF cavities are providing longitudinal focusing to the beam, generating bunches of particles (see the left-hand side of fig. 3).

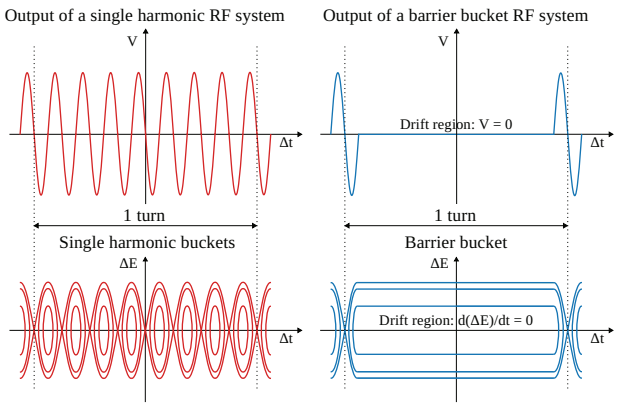

Fig. 3: Comparison of a single-harmonic waveform and corresponding longitudinal phase space (left) and a barrier bucket waveform and corresponding phase space (right).

A single RF bucket can be generated using an isolated sine pulse. However, if the voltage of the RF waveform is inverted, a long, flat bucket all along the circumference of the ring will be created (see the right-hand side of fig. 3). This is called a barrier bucket [15]. The main characteristic of a barrier bucket is that the confined particles can drift freely, as in an unbunched beam, between the two potential barriers. The basic description of the particle

dynamics in a barrier bucket can be obtained by considering the Hamiltonian describing the synchrotron motion of a single particle when an arbitrary RF voltage, $V(t)$, is applied to an accelerating RF cavity, namely [26,27]

$$H(\Delta E, \Delta t) = \frac{\eta}{2\beta^2 E_0}\Delta E^2 - \frac{1}{T_0}\int_0^{\Delta t} eV(\tau)\mathrm{d}\tau, \qquad (1)$$

where T_0 is the revolution period of the particles having E_0 energy, which is taken to be constant in this application. $\eta = 1/\gamma_{\mathrm{tr}}^2 - 1/\gamma^2$ is the slip factor (γ is the relativistic quantity and γ_{tr} is the value of γ corresponding to the transition energy), e is the elementary charge, and β is the relativistic factor. ΔE is the energy deviation with respect to E_0 and Δt is the difference in the arrival time of the particle with respect to the beginning of each turn. A few trajectories corresponding to a constant value of H have been plotted for two different RF waveforms in fig. 3 (bottom).

The main feature of a barrier bucket is that off-energy particles do not experience any change in ΔE during their drift between the potential barriers. This can be achieved if the RF voltage is zero in this drift region (see fig. 3, right). The second condition is that the RF waveform must be DC-free [15]. Apart from these two conditions, the actual shape of the V-pulse is a free parameter. The highest potential for a given amplifier peak output can be achieved by a rectangular pulse, but such a pulse requires a high-bandwidth RF system. In practice, the input waveform can be optimised as a trade-off between the depth of the potential well and the bandwidth used. The freedom in defining the shape of the waveform allows even to create so-called thick barrier buckets with systems having a lower bandwidth [28]. Note that waveform requirements for accelerating barrier buckets are not considered here, justified by the fact that beam loss reduction at constant energy in conjunction with the MTE process has been the main motivation for this study.

In order to generate a barrier bucket to further reduce the extraction losses for MTE, a wideband RF cavity, which has been installed in the PS ring in 2014 [29] (see fig. 2) as part of a longitudinal feedback, can be used. The cavity is loaded with Finemet® material, which makes it usable in the frequency range from 400 kHz to well above 10 MHz.

Since the system made of the cavity and its amplifier modifies the phase and the magnitude of the harmonics of the input signal in a non-uniform way, a pre-distortion scheme of the input waveform had to be developed to achieve the desired output. Indeed, applying the ideal waveform directly at the input of an RF system is usually not sufficient to produce a reasonably flat longitudinal beam distribution between the potential barriers [16,30]. A better waveform quality can be achieved by linearising the response of the RF system [31]. In particular, beam manipulations that require a changing barrier potential, such as compression, multiple injections, momentum mining [17] or more sophisticated operations, usually ask for precise control of the flatness of the beam density in the drift region of the barrier bucket. This can be obtained by applying small corrections to the drive signal [32].

To achieve the required precision in the waveform synthesis and facilitate a flexible implementation that allows the parameters of the barrier waveform to be easily programmed, an arbitrary shape, beam synchronous, signal generator based on programmable logic (FPGA) has been developed. The input waveform to the amplifier and the cavity can be calculated in a higher-level programming language (Python) based on high-resolution measurements of the cavity frequency response. Although fitting a single polynomial to approximate the wide-band transfer function was found to be a good approximation of the global system response, a combined, narrow-band interpolation approach in the relevant frequency range lead to a more precise barrier-bucket generation.

A number of tests has been performed in the PS as part of the initial validation with beam of the new RF gymnastics. These tests included measurements at injection energy and with different beam intensities, in order to disentangle the effects related to the response of the RF system from those due to beam-induced contributions. A quasi-constant beam density after optimising the already linearised waveform was achieved.

Experimental and simulation results. – The transverse beam splitting at the heart of MTE is performed at constant beam momentum of 14 GeV/c [1–4]. Before and during the splitting process, the beam is longitudinally confined into 16 RF buckets by the 10 MHz main RF system of the PS [33]. Prior to extraction, the voltage is normally reduced to zero and the beam is debunched. In order to facilitate the handover from the main RF system to the wideband one for the barrier bucket tests, the voltage of the main RF system is gradually lowered while the voltage of the barrier bucket system is increased. The phase of the gap created by the barrier bucket system is centred between two main RF buckets. An example of the debunching from standard buckets into a barrier bucket is shown in fig. 4.

The gradual disappearance of the bunches is clearly visible, with a symmetric gap appearing simultaneously in the empty space between two bunches. A scan was performed to synchronise the position of the barrier bucket with the rise time of the fast dipoles so to minimise extraction losses. After having completed this preliminary setting up, the longitudinal beam density has been measured both in the PS ring just prior to extraction as well as in the transfer line between the PS and SPS, and the results are shown in fig. 5. In the upper part the beam distribution along the PS circumference is shown a few turns before extraction. The gap generated by the barrier bucket is clearly visible and the distribution in the drift space between the RF barriers is reasonably flat. In the lower part, the longitudinal distribution is shown over five turns as a result of the transverse splitting. The single gap visible

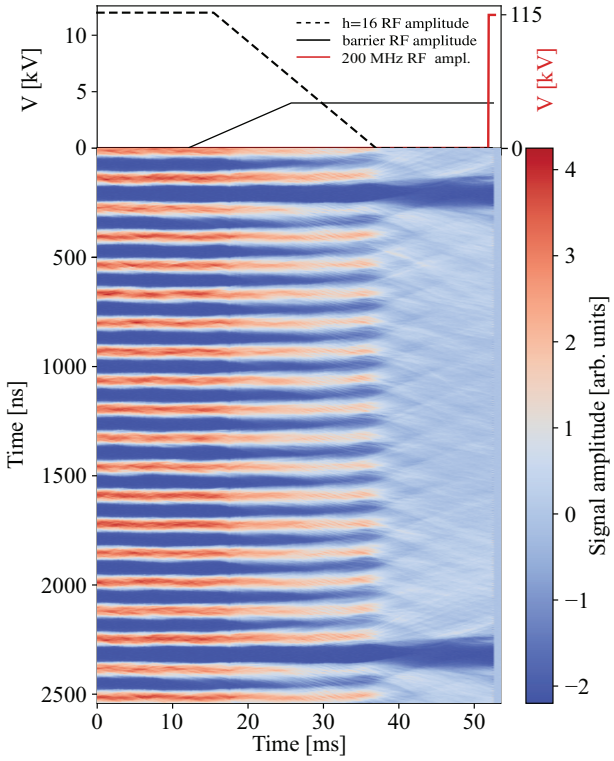

Fig. 4: Re-bucketing into a barrier bucket at total beam intensity of 1.87×10^{13} p. The voltage of the main accelerating RF system is lowered and simultaneously that of the wide-band system is increased. Finally, the amplitude of the 200 MHz system is raised within about 1 ms to reach full voltage at extraction. The vertical time axis represents a little more than one PS turn, $T_0 = 2.1\,\mu$s. The colour scale represents the longitudinal line density.

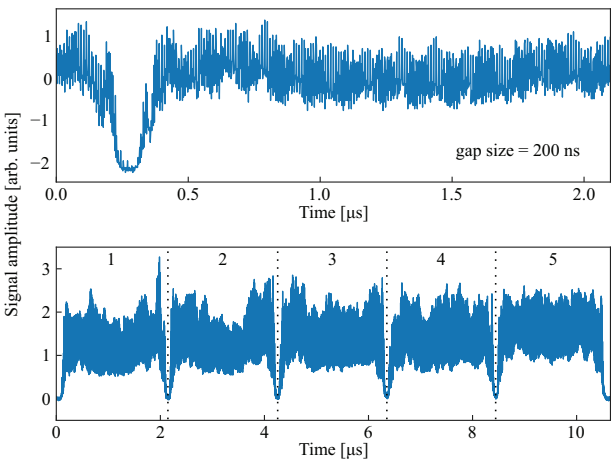

Fig. 5: Longitudinal beam profile measured in the PS prior to extraction (top) and after extraction in the transfer line between PS and SPS (bottom). Note the five-turn structure in the transfer line, which is generated by MTE. The gaps generated by the barrier buckets are clearly visible. The high-frequency modulation is generated by a 200 MHz RF system in the PS, which is required by the SPS to receive the beam correctly.

in the distribution in the PS ring is replicated four times and also in this case the distribution is reasonably flat between the gaps. Note that the high-frequency oscillations are generated by the 200 MHz RF system that is used to modulate the longitudinal beam density. Additional optimisation of the waveform of the barrier bucket should be performed to improve the flatness of the longitudinal beam distribution, but this is a second-order effect and has no impact on the losses at PS extraction. Note that the low-frequency modulation is present in MTE beams without the barrier bucket and its origin is being actively investigated and represents a coupling between transverse and longitudinal motion.

In addition, the longitudinal beam quality shows less degradation than expected [16] during the whole process. Qualitatively, the absence of major longitudinal blow-up can be deduced from the smooth evolution of the bunch profile during the re-bucketing process from 16 bunches into the barrier bucket (see fig. 4), with only a minor fraction of the beam remaining partially bunched.

For the quantitative evaluation of the longitudinal emittance and to analyse the bunch distribution at extraction, numerical simulations with the longitudinal tracking code BLonD [34] have been performed. They cover the re-bucketing from the conventional bunches in the main RF system at $h = 16$ into the barrier bucket. The pulsed RF voltage generating the barrier bucket has been modelled by the Fourier sum of 25 RF systems with sinusoidal amplitudes. The same algorithm was applied to synthesise the waveform used for the beam tests. The time evolution of voltages used in the tracking simulations corresponds to the ones illustrated in fig. 4. Intensity effects are not taken into account in these simulations.

The particle distribution in the longitudinal phase space and its corresponding emittance during acceleration can be reconstructed based on an ensemble of bunch profiles using tomography [35]. This measurement provides the initial emittance of the simulated bunches. The total emittance of all 16 bunches amounts to about 24 eVs. A minor longitudinal blow-up, below 10%, can be expected from the moment of the emittance measurement and the start of the re-bucketing process to the barrier bucket. Figure 6 shows the simulated evolution of the bunch profiles under conditions comparable to those of the measured evolution presented in fig. 4.

Figure 7 illustrates the resulting phase-space distribution of the particles in the barrier bucket at extraction, but without the modulation at 200 MHz, which is usually present only during the last few hundred turns. Due to the slow synchrotron motion, only a fraction of the particles is yet reflected at the barriers. This explains the shoulders of higher density observed at the edges of the final bunch.

The longitudinal emittance of the initial bunches was scanned in simulations to match the measured duration of the region without beam. Figure 8 shows that the simulated duration of the particle-free region agrees well with the measured one assuming an initial longitudinal

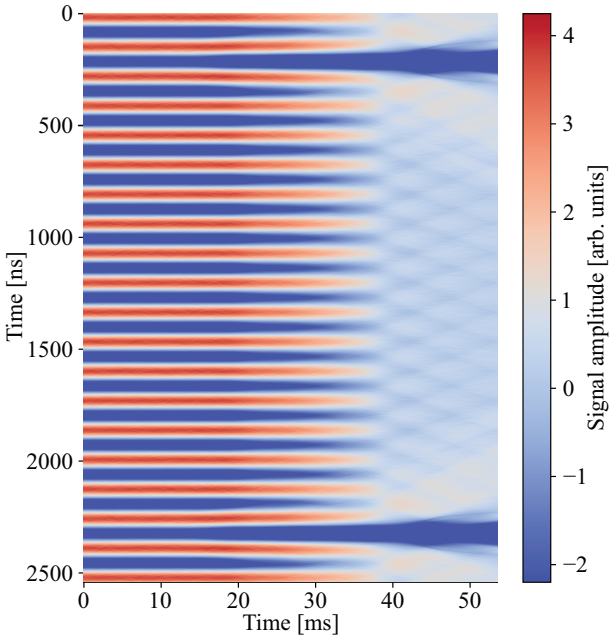

Fig. 6: Simulated profile evolution for the same principal RF voltage evolution as for the measurements shown in fig. 4. The initial longitudinal emittance corresponds to the one measured during acceleration.

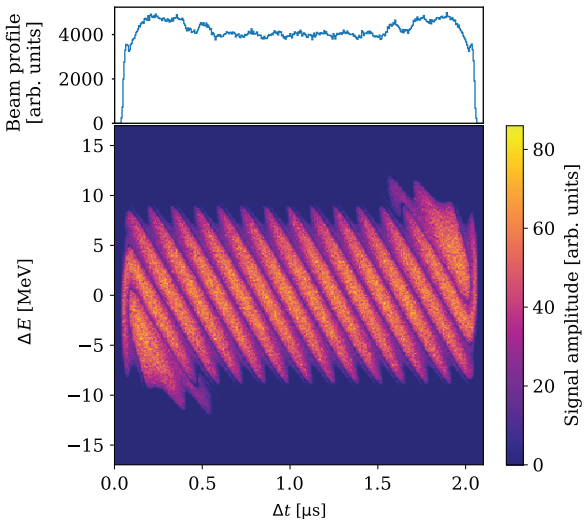

Fig. 7: Simulated longitudinal phase space at extraction with the matched emittance corresponding to figs. 4, 6 and without the 200 MHz modulation. The partial filamentation mechanism in the barrier bucket is illustrated. The projection of the beam distribution is also shown.

emittance of about 25 eVs. This is compatible with the total emittance measured during acceleration.

Although further studies with beam are required to assess the longitudinal emittance blow-up in more detail, fig. 7 indicates that the particles are merely redistributed in the central part of the barrier bucket as compared to a fully debunched beam. The time of the beam manipulation is too short for macroscopic emittance growth due to dilution.

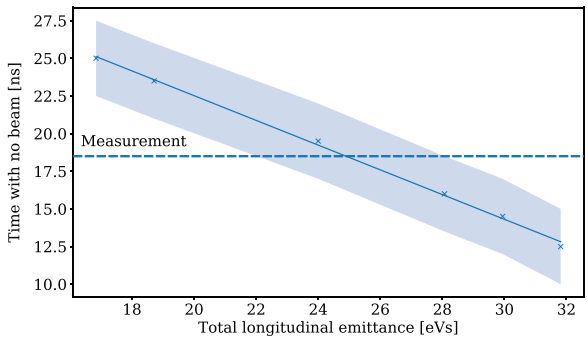

Fig. 8: Simulated duration of the particle-free region *vs.* total longitudinal emittance. The uncertainty in determining this time (±2.5 ns, light blue area) is dominated by the shape of the projections of the simulated bunch distribution.

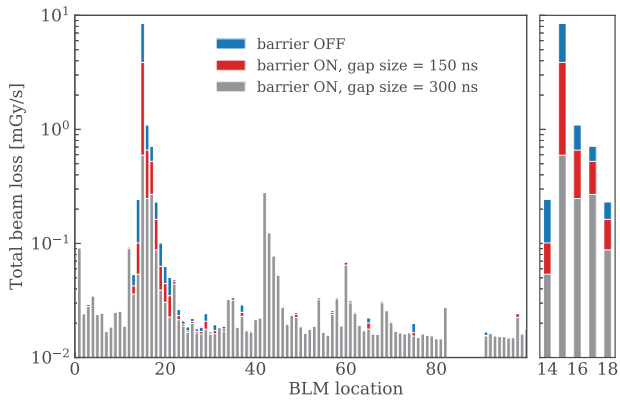

Fig. 9: Left: readings of the BLMs distributed along the PS ring for three different gap configurations. The dramatic reduction of losses in the extraction region is clearly visible. Right: zoom of the BLM readings in the extraction region.

The key measurements of these studies have been performed by assessing the impact of the gap in the longitudinal beam distribution on the extraction losses. Beam loss monitors (BLMs) are installed all along the PS ring. These devices are ionisation chambers and their technology is derived from the corresponding devices installed in the CERN LHC [36]. The comparison between various configurations is illustrated in fig. 9. The distribution of losses around the whole PS circumference is shown (left) together with a zoom (right) of the extraction region, corresponding to the location around the straight section 16 (see also fig. 2), where the highest peaks occur. This is the only ring location where the presence of the gap should induce a reduction of beam losses. The reduction of losses due to the presence of the gap is clearly visible. In agreement with expectations, a further reduction of beam losses is obtained by increasing the gap size.

A detailed scan of the gap width has been performed and the corresponding impact on the extraction losses is shown in fig. 10. Three different intensity regimes have been probed, namely the operational intensity used during the 2018 fixed-target physics run, an intermediate

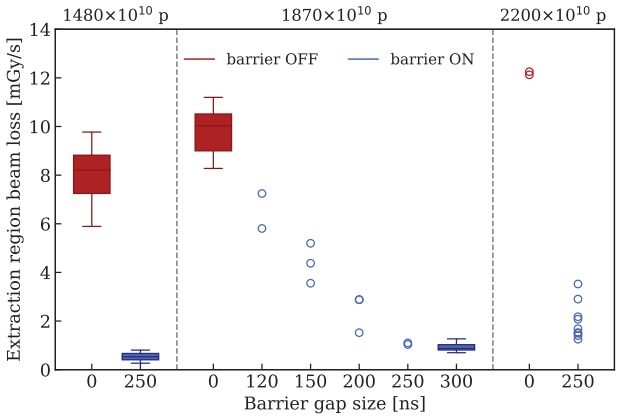

Fig. 10: Extraction losses as a function of the barrier gap size for three different total beam intensities (indicated on top of the plot). The extraction losses decrease dramatically due to the presence of the gap and a dependence on the gap width is evident. Boxes indicate the data distribution whenever more than 10 measurements are available for a given configuration.

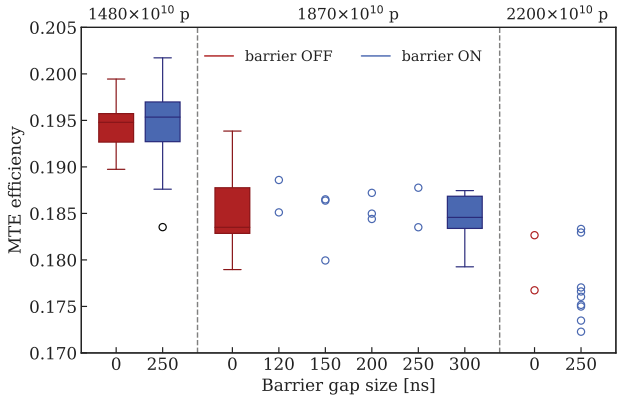

Fig. 11: MTE efficiency as a function of the barrier gap size for three different total beam intensities (indicated on top of the plot). No relevant impact of the gap presence on η_{MTE} is observed. The difference in η_{MTE} for different intensities is explained by the lack of time to adjust the splitting process during the measurements. Boxes indicate the data distribution whenever more than 10 measurements are available for a given configuration. The black open circle corresponds to an outlier.

intensity used for these special tests, and a high-intensity case, close to the value expected for future experiments (see, for example, the Search for Hidden Particles (SHiP) experiment [37]). For the high-intensity case, only a single value of the gap width has been tested. The analysis shows that a gain of a factor of 10 in losses can be achieved for a gap width of 300 ns. This excellent result does not depend on the total beam intensity, indicating that the barrier bucket gymnastics works very well in a rather extended intensity range.

These extremely promising results indicate that the sophisticated manipulations performed in the horizontal and longitudinal phase spaces are well decoupled from each other and also from the value of the total beam intensity. In addition, the use of the natural figure of merit of the MTE performance, namely

$$\text{MTE efficiency} = \eta_{\mathrm{MTE}} = \frac{\langle I_{\mathrm{Islands}} \rangle}{I_{\mathrm{Total}}}, \qquad (2)$$

where $\langle I_{\mathrm{Islands}} \rangle$ and I_{Total} stand for the average intensity in the islands and the total beam intensity, respectively, can provide a quantitative indication about the real decoupling between horizontal and longitudinal degrees of freedom. The nominal efficiency is 20% and corresponds to an equal beam sharing between islands and core. In fig. 11 the comparison of η_{MTE} for the three values of total beam intensity already considered is shown and it is clearly visible that the presence of the gap does not lead to significant differences in η_{MTE}. For the highest beam intensity a lack of statistics can be observed, which is due to the limited time available for these measurements. Nevertheless, the performance in terms of η_{MTE} appears to be comparable, but will certainly be subject of additional studies in the future. All in all, the presented results indicate a rather high degree of decoupling between the two complicated beam manipulations under study.

Conclusions. – Two original techniques have been merged into a single, novel, and highly sophisticated beam manipulation, whose successful studies have been reported in this article. A detailed experimental campaign has been carried out in 2018 to assess the performance of the barrier bucket technique in the PS and its application in conjunction with the MTE process. The goal of reducing the beam losses virtually to zero at PS extraction has been successfully achieved, which is an essential step in view of future high-intensity fixed-target experiments at the SPS, such as SHiP. To implement the loss-free transfer, the longitudinal gap generated by the barrier bucket still needs to be aligned in time with a beam already circulating in the SPS. This will be subject to future studies. First longitudinal beam dynamics simulation studies without intensity effects confirm the basic features of the observed profile evolution. These simulations also suggest that the barriers change the longitudinal beam distribution near the gap only, due to the short duration of the manipulation. The detailed analysis of the SPS ring performance for MTE beams in combination with the barrier bucket is in progress with the goal of quantitatively assessing the overall performance of this new and highly advanced beam process.

REFERENCES

[1] Cappi R. and Giovannozzi M., *Phys. Rev. Lett.*, **88** (2002) 104801.
[2] Borburgh J. *et al.*, *EPL*, **113** (2016) 34001.
[3] Abernethy S. *et al.*, *Phys. Rev. Accel. Beams*, **20** (2017) 014001.
[4] Huschauer A. *et al.*, *Phys. Rev. Accel. Beams*, **20** (2017) 061001.
[5] Huschauer A. *et al.*, *J. Phys.: Conf. Ser.*, **874** (2017) 012072.

[6] Bovet C. *et al.*, *IEEE Trans. Nucl. Sci.*, **20** (1973) 438.
[7] Fiander D. C., Grier D. *et al.*, *IEEE Trans. Nucl. Sci.*, **24** (1977) 1340.
[8] Gilardoni S. *et al.*, *Phys. Rev. ST Accel. Beams*, **9** (2006) 104001.
[9] Franchi A., Gilardoni S. and Giovannozzi M., *Phys. Rev. ST Accel. Beams*, **12** (2009) 014001.
[10] Bartosik H. *et al.*, in *IPAC 2012*, edited by Eyberger C. and Zimmermann F. (IEEE Computer Society Press, Piscataway) 2012, p. 499.
[11] Gilardoni S. *et al.*, in *IPAC 2012*, edited by Eyberger C. and Zimmermann F. (IEEE Computer Society Press, Piscataway) 2012, p. 502.
[12] Hernalsteens C. *et al.*, in *IPAC 2013*, edited by Dai Z. *et al.* (JACoW, Geneva) 2013, p. 2633.
[13] Hernalsteens C. *et al.*, in *IPAC 2013*, edited by Dai Z. *et al.* (JACoW, Geneva) 2013, p. 2636.
[14] Bertone C. *et al.*, CERN-ACC-2014-0043 (2014).
[15] Griffin J. E. *et al.*, *IEEE Trans. Nucl. Sci.*, **30** (1983) 3502.
[16] Fujieda M. *et al.*, *Phys. Rev. ST Accel. Beams*, **2** (1999) 122001.
[17] Bhat C. M., *Phys. Lett. A*, **330** (2004) 481.
[18] Takayama K. *et al.*, *Phys. Rev. Lett.*, **94** (2005) 144801.
[19] Takayama K. *et al.*, *Phys. Rev. Lett.*, **98** (2007) 054801.
[20] Gilardoni S., Giovannozzi M. and Hernalsteens C., *Phys. Rev. ST Accel. Beams*, **16** (2013) 051001.
[21] Machida S. *et al.*, *Phys. Rev. Accel. Beams*, **20** (2017) 121001.
[22] `http://pbc.web.cern.ch`.
[23] Jaeckel J., Lamont M. and Vallee C., CERN-PBC-REPORT-2018-003, arXiv:1902.00260 (2018).
[24] Burnet J.-P. *et al.*, CERN-2011-004 (2011).
[25] Persichelli S. *et al.*, in *IPAC 2014*, edited by Petit-Jean-Genaz C. *et al.* (JACoW, Geneva) 2014, p. 1708.
[26] Dome G., CERN-1984-015 (1983), p. 215.
[27] Lee S. Y. and Ng K. Y., *Phys. Rev. E* **55** (1997) 5992.
[28] Bohl T., Linnecar T. and Shaposhnikova E., CERN SL-Note-2000-032 (HRF) (2000).
[29] Paoluzzi M. and Damerau H., CERN-ACC-NOTE-2013-0019 (2013).
[30] Bohl T., Linnecar T. and Shaposhnikova E., CERN-SL-2000-020 (HRF) (2000).
[31] Dey J. *et al.*, in *PAC 2003*, edited by Chew J. *et al.* (IEEE Computer Society Press, Piscataway) 2003, p. 1204.
[32] Crisp J. *et al.*, KEK-PROCEEDINGS-2006-15, HB 2006 (KEK, Tsukuba) 2006, p. 244.
[33] Favia G. *et al.*, in *IPAC 2016*, edited by Petit-Jean-Genaz C. *et al.* (JACoW, Geneva) 2016, p. 622.
[34] CERN Beam Longitudinal Dynamics code BLonD, `http://blond.web.cern.ch`.
[35] Hancock S., Knaus P. and Lindross M., in *EPAC 1998*, edited by Petit-Jean-Genaz C. *et al.* (JACoW, Geneva) 1998, p. 1520.
[36] Damerau H. *et al.*, CERN-ACC-2014-0337 (2014), p. 593.
[37] De Lellis G., *Nucl. Part. Phys. Proc.*, **263-264** (2015) 71.